WARSAW UNIVERSITY OF TECHNOLOGY Index 351733
FACULTY OF CIVIL ENGINEERING
COMMITTEE FOR CIVIL AND WATER ENGINEERING
POLISH ACADEMY OF SCIENCES ISSN 1230-2945

DOI: 10.24425/ace.2023.146074

ARCHIVES OF CIVIL ENGINEERING

Vol. LXIX ISSUE 3 2023

pp. 173 –185

Research paper

Dynamic performance of bridge piers impacted by heavy trucks

Yao Huang[1]

Abstract: Vehicle-bridge collision accidents often result in significant economic losses and negative social effects, with heavy trucks being the most destructive to bridge structures. Therefore, this study uses a high-precision finite element method to investigate the impact resistance of concrete bridge piers when subjected to heavy truck impact. The main conclusions of this paper are as follows: (1) When heavy trucks collide with bridge piers, two peak impact forces are generated due to engine and cargo collisions. The peak collision force generated by engine impact is 17.7% greater than that generated by cargo impact. (2) The damage to the bridge, when impacted by heavy trucks, is mainly concentrated on the affected pier. The primary damage characteristics of the bridge piers include punching shear damage at the impact point, tensile damage at the backside, and shear damage at the pier top. (3) The peak values of shear force and bending moment both appear at the bottom of the pier, and the combination of the two causes serious flexural-shear failure damage at the bottom of the pier. (4) The axial force is fluted along the pier height, and the axial force at the top and bottom of the pier is the largest, while the axial force at the middle section is relatively small. The instantaneous axial force of bridge pier will reach more than 2 times the axial force during operational period, seriously threatening the safety of bridge. Overall, this study provides valuable insights into the impact resistance of concrete bridge piers when subjected to heavy truck impact, which can help engineers and policymakers in designing more robust and safer bridges.

Keywords: heavy truck, vehicle-bridge impacts, finite element method, anti-impact performance

[1]MSc., Eng., Nanning College of Technology, Guangxi, 541006, China, e-mail: huangyao_2022@163.com, ORCID: 0000-0001-6960-1822

1. Introduction

The frequent accidents of vehicles colliding with bridges cause damage to the bridge structure, and even result in the collapse of the entire bridge structure, causing significant loss of life, massive economic losses, and negative social impacts. Heavy trucks are particularly destructive in such accidents, often causing structural failure and collapse of bridges. Buth et al. reported that out of 19 cases of heavy truck collisions with bridge piers in the United States, four resulted in the collapse of the entire bridge structure [1]. According to online reports, at least 16 cases of heavy truck collisions with bridge piers occurred in China between July 2018 and December 2019, including one bridge collapse and three pier failures. The above data shows that concrete bridge structures exhibit a significant lack of collision resistance under the strong impact of heavy trucks.

Equivalent static load is often used as the design criterion of bridge impact resistance, but this method ignores differences in the materials of the collided piers, the colliding vehicles, and the boundary conditions. In addition, different countries have significant differences in the regulations for this static load value [2,3]. Therefore, the dynamic solution and design problems of vehicle-bridge collisions have always been a concern of scholars worldwide. Over the past 30 years, experimental, theoretical, and finite element methods have been the three main methods for solving vehicle-bridge collision problems [4–8]. Among them, the experimental method is the most reliable but is costly, and full-scale testing requires enormous manpower and material resources, so there are relatively few full-scale testing studies currently conducted domestically and abroad [9–12]. Although the theoretical method is less expensive, it is difficult to consider many influencing factors at the same time due to the material nonlinearity, geometric nonlinearity, and boundary nonlinearity involved in vehicle-bridge collisions [11, 12]. Finite element methods are widely used due to their low cost and high solving accuracy with appropriate parameter selection and model settings [13–16].

In this paper, a high-resolution truck-bridge collision model is built based on LS-DYNA, and the collision model is validated. Based on the high-precision dynamic finite element method, this paper studied the impact resistance of concrete bridge piers under high-speed collision by heavy trucks. The research mainly includes the following aspects: the collision force characteristics of heavy trucks and bridge piers, the damage characteristics of bridge piers, and the dynamic response of the bridge structure.

2. Truck-bridge collision model

2.1. Meshing strategy

The vehicle model used in this article is the Ford 800 truck, with a total weight of 16 tons. The model is discretized using beam, solid, and shell elements, with a total of 35,297 elements and 7 types of materials. The truck model has a Detroit DD15 14.8-L engine, which has a weight of 14 kN and is simulated by *MAT_ELASTIC. The fully-

integrated solid element (ELFORM = 2) is adopted by the engine. The cargo is modeled by *MAT_SOIL_AND_FOAM with a density of 1800 kg/m^3 and a shear modulus of 50.4 MPa. The research object is a 3 × 20 m simply supported T-beam bridge on the Yongjin Expressway, with a 20 m span and a 7.6 m wide deck. The lower structure consists of double-column bridge piers, with a height of 6.3 m and a diameter of 1.5 m, as shown in Fig. 1. The AUTO_CONTACT_SURFACE_TO_SURFACE keyword is used to simulate the collision between the vehicle and the bridge piers. To improve the computational efficiency of explicit analysis, an 8-node solid element with a single integration point is used to simulate the bridge piers, bearings, cover beams, upper structures, bridge abutments, and supports [16]. Beam elements are used to simulate longitudinal and transverse reinforcement embedded in the pier columns. The relationship between the reinforcement and the concrete is assumed to be fully bonded, and is implemented using the keyword CONSTRAINED_LAGRANGE_IN_SOLID. The gravity of the impact model is simulated by *LOAD_BODY_Z keyword. The established finite element model is shown in Fig. 2.

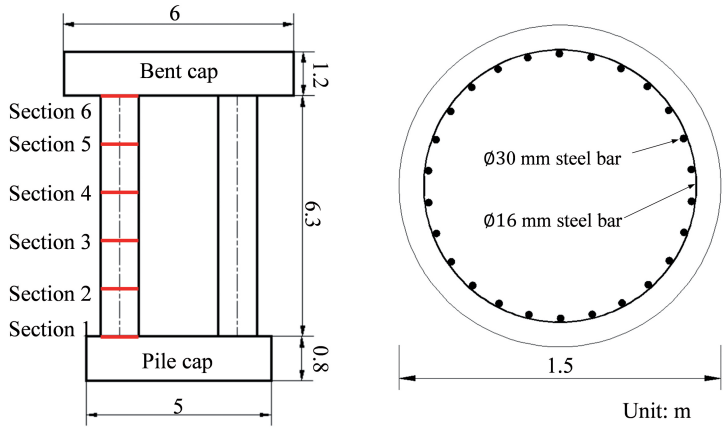

Fig. 1. Diagram of the bridge pier

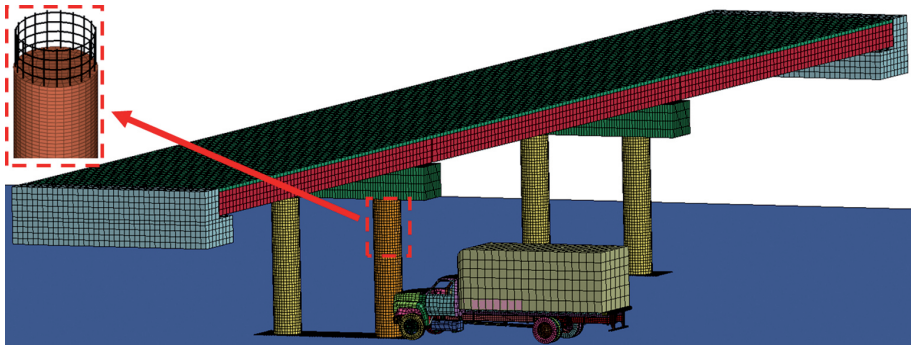

Fig. 2. Truck-bridge collision model

2.2. Material

The model uses the Continuous Surface Cap Model (MAT_159) to simulate the mechanical behavior of concrete [16]. The yield surface of MAT_159 is represented as follows:

$$f(J_1, J_2, J_3, \kappa) = J_2 - R^2 F_f^2 F_C \tag{2.1}$$

where J_1, J_2, and J_3 are the three stress sensor invariants. κ is the cap hardening parameter, R is the reduction function, F_f and F_C are the shear failure surface and the cap hardening function, respectively. The uniaxial compressive strength of the concrete used in this paper is 40 MPa. The Continuous Surface Cap Model provides a method to automatically generate material parameters by inputting the compressive strength of the material prism.

Steel bars are modelled using MAT_PLASTIC_KINEMATIC, and the strain rate effect is calculated using Cowper–Symonds law. The yield stress is:

$$\sigma_y = \left[1 + \left(\frac{\dot{\varepsilon}}{C}\right)^{\left(\frac{1}{P}\right)}\right]\left(\sigma_0 + \beta E_p \varepsilon_{\text{eff}}^p\right) \tag{2.2}$$

where σ_0 is the initial yield stress, $\dot{\varepsilon}$ is the strain rate, $\varepsilon_{\text{eff}}^p$ is the effective plastic strain, β is the hardening rule parameter; C and p are the strain rate parameters of Cowper–Symonds, and E_p is the plastic hardening modulus.

$$E_p = \frac{E_t E}{E - E_t} \tag{2.3}$$

where E represents the elastic modulus of the steel reinforcement; E_t represents the tangent modulus.

2.3. Model validation

Based on the concrete beam drop hammer impact test conducted by Fujikake [6], the NC material model **is** validated. Beam S1616, with longitudinal bars with a diameter of 16 mm, is selected for validation (drop height of 1.2 m). Fig. 3 shows the comparison

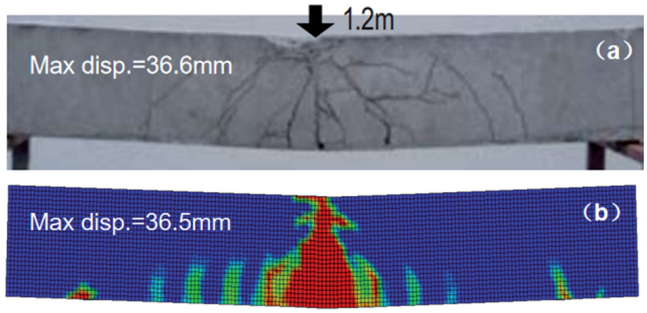

Fig. 3. Damage distribution: (a) S1616 beam; (b) numerical result

of damage between simulation results and experimental results, while Fig. 4 shows the comparison of collision force and mid-span displacement time history curves. As shown in Fig. 3, the finite element model and the test beam both exhibit tensile cracking in the mid-span region and similar concrete punching damage at the impact point, indicating that the finite element model can reasonably predict bending cracks near the impact point and damage to the impact surface. As shown in Fig. 4, the collision force and mid-span displacement time history curves of the finite element model exhibit consistent trends, and the values of the maximum impact force (308.4 kN, 310.9 kN) and mid-span maximum displacement (36.6 mm, 36.5 mm) are very close, indicating that the collision simulation method used in this study is reasonable.

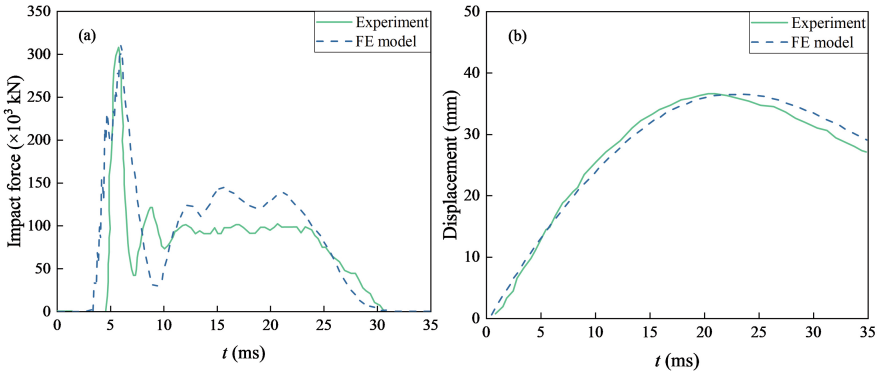

Fig. 4. Verification: (a) Impact force; (b) mid-span displacement

3. Results analysis

3.1. Characteristics of impact force

When a vehicle is driven on a highway, the speed can exceed 100 km/h. In the event of a collision, it causes a huge impact force on the bridge structure, which may lead to the collapse of the bridge. Therefore, to simulate the collision between a vehicle and a bridge pier, an initial speed of 120 km/h is applied to the truck to cause a head-on collision with the bridge pier. The collision process and the deformation of the truck are shown in Fig. 5. It can be seen that the main process of the collision between the heavy vehicle and the bridge pier is as follows: at $t = 0$ s, the vehicle starts to come into contact with the bridge pier, and at this time the vehicle is intact. The vehicle continues to move forward, and the front of the vehicle begins to be gradually compressed. At $t = 0.05$ s, the bumper of the vehicle comes into contact with the bridge pier. When $t = 0.07$ s, the front of the vehicle undergoes local deformation, and the truck engine comes into contact with the bridge pier. At $t = 0.16$ s, the front of the vehicle is completely compressed, the top of the vehicle compartment is deformed, the mechanical structure of the lower part of the vehicle is severely crushed, and the cargo comes into contact with the bridge pier.

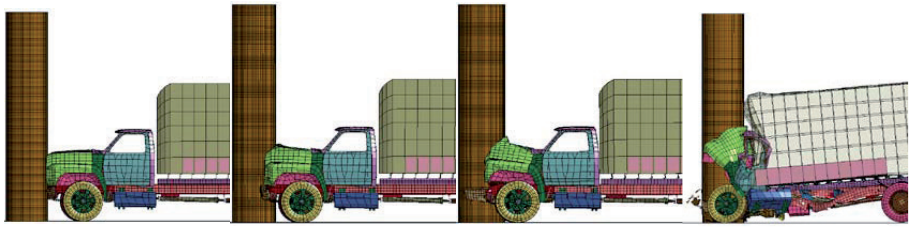

Fig. 5. Collision process

As shown in Fig. 6, the collision force-time curve is illustrated. The collision force starts to increase from $t = 0$ s, reaching its first peak at approximately 6.96×10^3 kN and then dropping to 0 kN at $t = 0.25$ s, with the entire collision process lasting approximately 0.25 s. It can be observed that the vehicle-bridge collision problem is an instantaneous dynamic problem, with a short duration of load but extremely destructive force. It can also be seen that when the bridge pier structure is hit by a heavy truck, the collision force exhibits two peaks (6.96×10^3 kN and 5.73×10^3 kN), respectively generated by the engine and cargo collisions. The peak collision force generated by engine impact is 17.7% greater than that generated by cargo impact. This is because the kinetic energy of the vehicle has been greatly reduced when the cargo hits the pier, thus causing a small collision force.

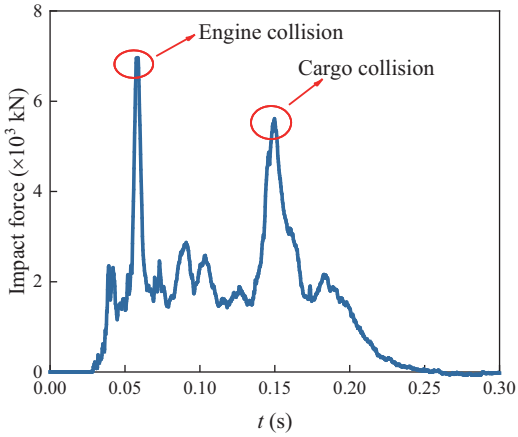

Fig. 6. Truck-pier impact force

3.2. Pier damage

The damage results of the bridge after the collision are shown in Fig. 7. The damage to the bridge is mainly concentrated on the impacted pier, while other parts are basically undamaged. The reason for this may be that the entire process of the vehicle-bridge collision

only lasts about 0.25 seconds, which is extremely short, and other components of the bridge cannot react in time. Fig. 8 shows the damage of the pier at different times, where the maximum plastic strain is used to represent the concrete damage, with a minimum value of 0 indicating no damage and a maximum value of 1 indicating concrete failure. It can be seen that as the time increases, the pier damage gradually gets worse. The main damage features of the pier are: impact-shear damage on the front face, tensile damage on the back

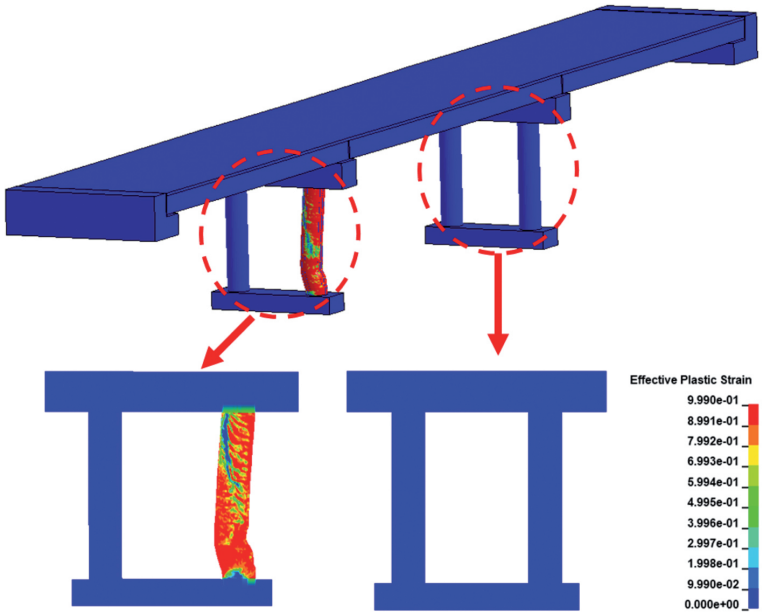

Fig. 7. Damage of the entire bridge

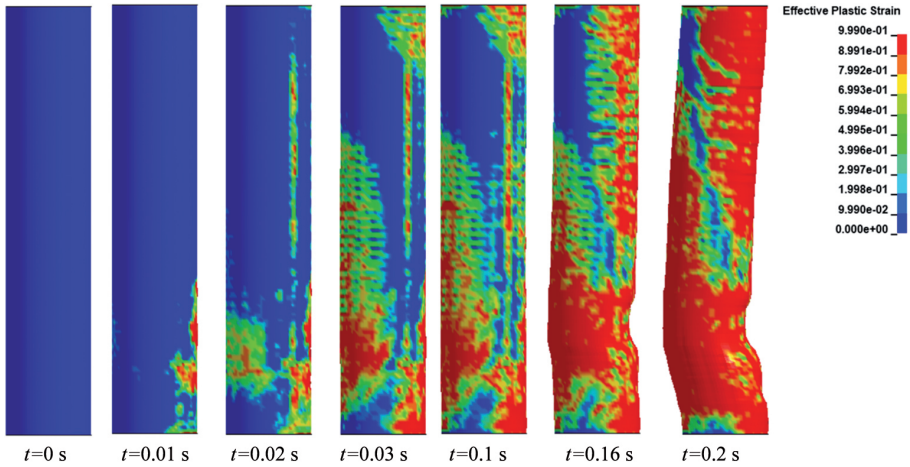

Fig. 8. Damage process of the bridge pier

face, and shear damage at the pier top. When $t = 0$ s, the vehicle not collides with the pier and no damage occurred. When $t = 0.01$ s, there is slight compression damage on the impact face of the pier. At $t = 0.02$ s, there is tensile damage on the back face of the pier, and a damage band from top to bottom appeared in the upper part of the pier, which is caused by the constraint effect of the upper structure due to the large tensile stress on the impact face. As the collision continues, the tensile area on the back face of the pier gradually increases, and obvious stripe-like damage can be seen on the back face of the pier due to the constraint effect of the hoops. Shear damage starts to appear at the top of the pier, and obvious flexural-shear failure damage appears on the impacted part. At $t = 0.2$ s, the impacted location of the pier undergoes significant horizontal displacement, and the bearing capacity of the pier may be drastically reduced at this time.

3.3. Displacement response of the pier

To further analyze the dynamic response of the bridge pier at each cross section, six cross sections are set up on the pier, as shown in Fig. 1. Fig. 9 shows the displacement time-history curves of each section of the bridge pier during the vehicle-bridge collision process. As shown in Fig. 9, the displacement of the pier base section (Section 1) remains at 0 mm because it is connected to the bearing. In addition to Section 1, the displacement of each section of the pier fluctuates with the collision action, and the fluctuation amplitude increases with height. The peak displacement of the pier top (Section 6) is higher than that of other sections, reaching 7.8 mm. This is because the upper part of the deck is in a free boundary state, but the constraint effect gradually weakens from bottom to top due to the adhesive action between materials and the equivalent mass constraint of the pier top.

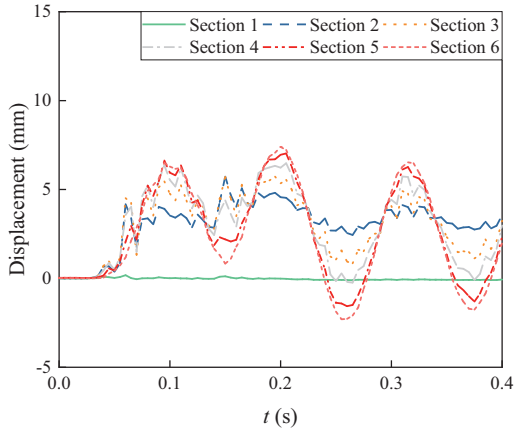

Fig. 9. Time history of displacement

The shear force-time history curves of each cross section are shown in Fig. 10. For comparison, the collision force-time history curve is also given in the figure. As can be seen from the figure, the peak shear forces of all bridge pier cross sections occur around the

time of the engine impact and cargo impact. Among them, the peak shear force of Section 1 (pier bottom) is closest to the engine collision force, and its direction is the same as that of the collision force. The peak shear force of Section 6 (pier top) is in the opposite direction to the engine collision force, which is the reason for the shear damage that occurred on the back of the struck bridge pier at the top of the pier (see Fig. 6). Fig. 11 further shows the distribution of the maximum shear forces for each cross section. As shown in Fig. 11, the location of the maximum shear force is at section 1, which is 430% higher than the shear force at cross section 2. This is the reason why the maximum shear damage of the bridge pier occurs at the base of the pier, and the design should protect the base of the pier.

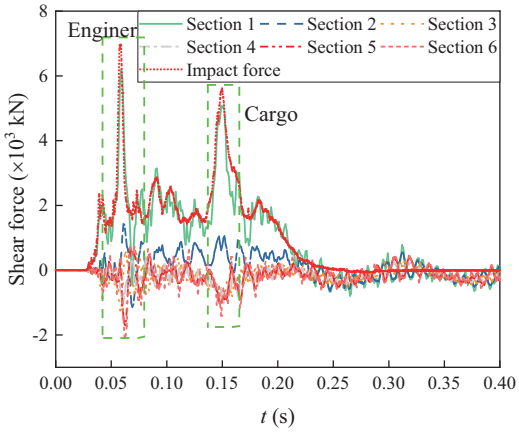

Fig. 10. Time history of shear force

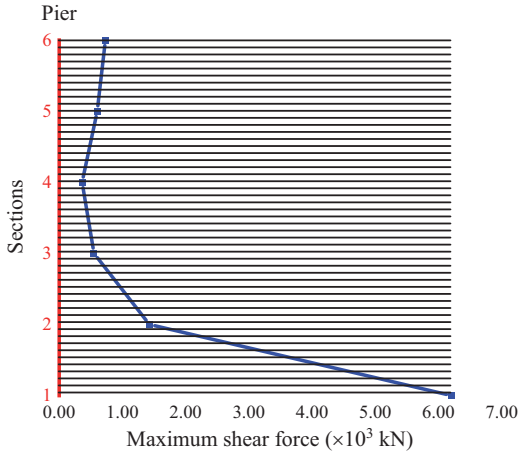

Fig. 11. Distribution of maximum shear force

The moment-time history curves of each cross section of the bridge pier during the vehicle-bridge collision process are shown in Fig. 12. Fig. 13 further shows the distribution

of the maximum moment values for each cross section. From Figs. 12 and 13, it can be seen that during the vehicle-bridge collision, the moment of each cross section of the bridge pier undergoes severe positive and negative fluctuations. Under normal operating conditions, the moment of the bridge pier should remain at 0. The maximum moment value of each cross section is distributed in a serrated pattern along the height direction of the bridge pier. Among them, the cross section with the largest moment peak is the base cross section (cross section 1), with a maximum value of 0.23×10^3 kN·m. The combined action of the base moment and shear force leads to the occurrence of base flexural-shear failure (see Fig. 8). At the same time, the positive moment values of the middle sections (Sections 3 and 4) are also large, causing tensile damage to the back of the bridge pier (see Fig 8).

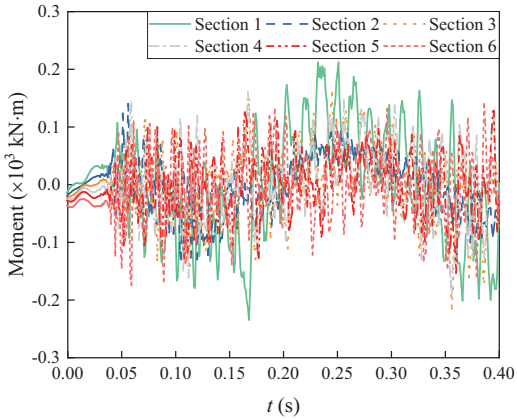

Fig. 12. Time history of moment

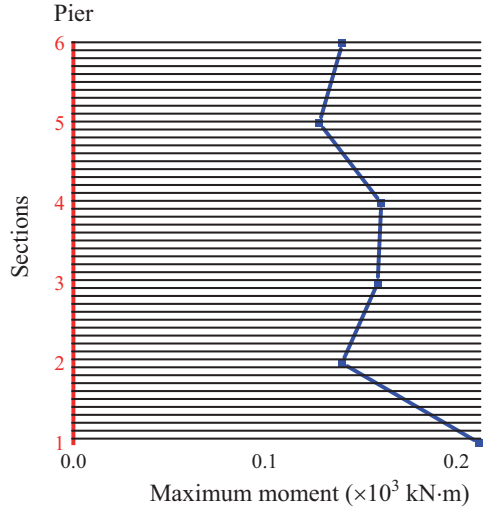

Fig. 13. Distribution of maximum moment

Under the action of impact force, when the deformation of the bridge pier is small, increasing the axial load can usually improve the impact resistance of the bridge pier. However, when the deformation of the bridge pier is large, increasing the axial load may cause the P-delta effect, which will reduce the axial bearing capacity of the bridge pier. Therefore, Fig. 14 shows the axial force-time history curves of each cross section of the bridge pier during the vehicle-bridge collision process, and Fig. 15 further shows the distribution of the maximum axial force values for each cross section. From Figs. 14 and 15, it can be seen that the axial force of the bridge pier is caused by the upper structure, and the axial force of each pier under normal operating conditions is about -2×10^3 kN.

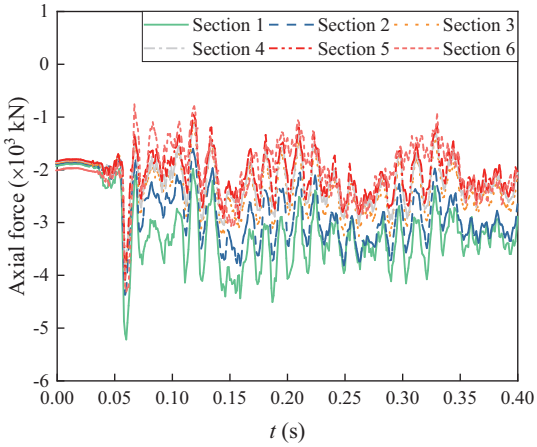

Fig. 14. Time history of axial force

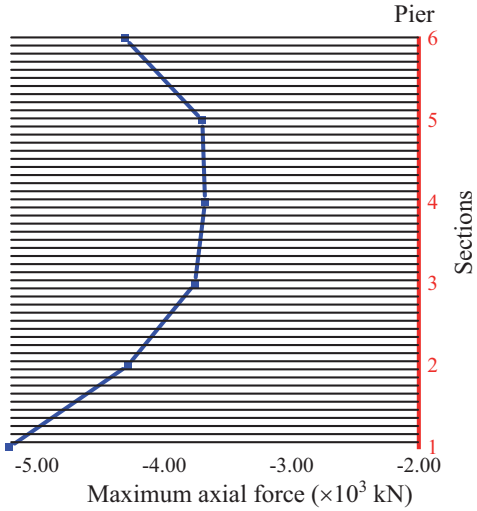

Fig. 15. Distribution of maximum axial force

The vehicle collision causes the axial force of the pier to fluctuate violently, deviating significantly from the normal operating axial force value. Among them, the axial force at the position of Section 1 (pier bottom) even reaches -5.32×10^3 kN, which is 2.7 times the normal operating axial force. The maximum axial force at Section 6 (pier top) is also large, reaching -4.42×10^3 kN, which is 2.2 times the normal operating axial force. The maximum axial force is at the pier top and pier bottom, and the axial force of the middle section is relatively small, that is, the axial force is concave along the height direction of the pier. These phenomena indicate that when the bridge pier is subjected to a heavy truck impact, the instantaneous axial force of the pier will exceed twice the normal operating axial force, completely breaking the original equilibrium state of the pier under load and posing a serious threat to the safety of the bridge.

4. Conclusions

1. When heavy trucks collide with bridge piers, two peak impact forces are generated due to engine and cargo collisions. The peak collision force generated by engine impact is 17.7% greater than that generated by cargo impact.
2. The damage to the bridge, when impacted by heavy trucks, is mainly concentrated on the affected pier. The primary damage characteristics of the bridge piers include punching shear damage at the impact point, tensile damage at the backside, and shear damage at the pier top.
3. The peak values of shear force and bending moment both appear at the bottom of the pier, and the combination of the two causes serious flexural-shear failure damage at the bottom of the pier.
4. The axial force is fluted along the pier height, and the axial force at the top and bottom of the pier is the largest, while the axial force at the middle section is relatively small. Instantaneous axial force of bridge pier will reach more than 2 times of the axial force under operational period, seriously threatening the safety of bridge.

References

[1] C.E. Buth, M.S. Brackin, W.F. Williams, and G.T. Fry, "Collision loads on bridge piers: phase 2, report of guidelines for designing bridge piers and abutments for vehicle collisions", TTI: 9-4973-2. Texas Transportation Institute, 2011.

[2] Ministry of Transport of the People's Republic of China, *General specifications for design of highway, JTG D60—2015[S]*. Beijing: China Communications Press, 2015.

[3] *AASHTO LRFD Bridge Design Specifications*. Washington: American Association of State Highway and Transportation Officials, 2013.

[4] W. Fan, B. Liu, and G.R. Consolazio, "Residual capacity of axially loaded circular RC columns after lateral low-velocity impact", *Journal of Structural Engineering*, vol. 145, no. 6, 2019, doi: 10.1061/(asce)st.1943-541x.0002324.

[5] W. Fan, X. Xu, Z. Zhang, and X. Shao, "Performance and sensitivity analysis of UHPFRC-strengthened bridge columns subjected to vehicle collisions", *Engineering Structures*, vol. 173, pp. 251-268, 2018, doi: 10.1016/j.engstruct.2018.06.113.

[6] K. Fujikake, B. Li, and S. Soeun, "Impact response of reinforced concrete beam and its analytical evaluation", *Journal of Structural Engineering*, vol. 135, no. 8, pp. 938-50, 2009, doi: 10.1061/(asce)st.1943-541x.0000039.

[7] L. Buda-Ożóg, J. Zięba, K. Sieńkowska, and D. Nykiel, "Influence of the tie reinforcement on the development of a collapse caused by the failure of an edge column in RC flat slab system", *Archives of Civil Engineering*, vol. 69, no. 1, pp. 39-54, 2023, doi: 10.24425/ace.2023.144158.

[8] M. Kiraga, S. Bajkowski, and J. Urbański, "Bridge headwater afflux estimation using bootstrap resampling method", *Archives of Civil Engineering*, vol. 69, no. 1, pp. 21-37, 2023, doi: 10.24425/ace.2023.144157.

[9] R. Xie, W. Fan, B. Liu, and D. Shen, "Dynamic behavior and vulnerability analysis of bridge columns with different cross-sectional shapes under rockfall impacts", *Structures*, vol. 26, pp. 471-86, 2020, doi: 10.1016/j.istruc.2020.04.042.

[10] V.D. Tin, M.P. Thong, and H. Hao, "Proposed design procedure for reinforced concrete bridge columns subjected to vehicle collisions", *Structures*, vol. 22, pp. 213-29, 2019, doi: 10.1016/j.istruc.2019.08.011.

[11] Y. Shi, H. Hao, and Z.-X. Li, "Numerical derivation of pressure-impulse diagrams for prediction of RC column damage to blast loads", *International Journal of Impact Engineering*, vol. 35, no. 11, pp. 1213-1227, 2008, doi: 10.1016/j.ijimpeng.2007.09.001.

[12] D. Bertrand, F. Kassem, F. Delhomme, and A. Limam, "Reliability analysis of an RC member impacted by a rockfall using a nonlinear SDOF model", *Engineering Structures*, vol. 89, pp. 93-102, 2015, doi: 10.1016/j.engstruct.2015.01.051.

[13] Y. Yu, L. Deng, W. Wang, and C. S. Cai, "Local impact analysis for deck slabs of prestressed concrete box-girder bridges subject to vehicle loading", *Journal of Vibration and Control*, vol. 23, no. 1, pp. 31-45, 2017, doi: 10.1177/1077546315575434.

[14] X. Zhang, X. Wang, W. Chen, Z. Wen, and X. Li, "Numerical study of rockfall impact on bridge piers and its effect on the safe operation of high-speed trains", *Structure and Infrastructure Engineering*, vol. 17, no. 1, pp. 1-19, 2021, doi: 10.1080/15732479.2020.1730406.

[15] A. Ventura, V. De Biagi, and B. Chiaia, "Effects of rockfall on an elastic-plastic member: A novel compliance contact model and dynamic response", *Engineering Structures*, vol. 148, pp. 126-44, 2017, doi: 10.1016/j.engstruct.2017.06.046.

[16] Y.K. Liu, J. Yang, G.J. Xu, H. Wei, and E. Deng, "Performance of UHPC bridge piers subjected to heavy vehicle collisions and probability analysis of damage level", *Structures*, vol. 47, pp. 212-232, 2023, doi: 10.1016/j.istruc.2022.11.061.

Received: 2023-2-21, Revised: 2023-06-07